

Appendices

Contents

Appendix A Impact parameter resolution for two layers.....	215
Appendix B The track equations	217
Appendix C Calculation of the helix parameters	221
Appendix D Loop corrections, renormalisation and fine-tuning.....	223
D.1 Feynman calculus	223
D.2 Feynman diagram of loop corrections.....	223
D.3 Renormalisation	223
D.4 Running masses and couplings	224
Appendix E Calculation of space-points	225
E.1 Introduction	225
E.2 Barrel SCT.....	225
E.3 End-cap SCT	225

Appendix A Impact parameter resolution for two layers

In this appendix the resolution of the impact parameters is deduced when two detector layers are used. In general for any $n \times n$ matrix \mathbf{M} given by:

$$\mathbf{M} = \begin{pmatrix} M_{11} & M_{12} & \cdots & M_{1n} \\ M_{21} & M_{22} & \cdots & M_{2n} \\ \vdots & \vdots & \vdots & \vdots \\ M_{n1} & M_{n2} & \cdots & M_{nn} \end{pmatrix} \quad (\text{A.1})$$

If \mathbf{M} is not singular one can find the inverse matrix $\mathbf{K} = \mathbf{M}^{-1}$ as:

$$\mathbf{K} = \frac{1}{\det \mathbf{M}} \begin{pmatrix} K_{11} & K_{12} & \cdots & K_{1n} \\ K_{21} & K_{22} & \cdots & K_{2n} \\ \vdots & \vdots & \vdots & \vdots \\ K_{n1} & K_{n2} & \cdots & K_{nn} \end{pmatrix} \quad (\text{A.2})$$

The term K_{jk} is the cofactor or adjunct determinant of M_{jk} in $\det \mathbf{M}$.

If the (r, ϕ) plane and the (r, z) plane are treated separately, the $(5 + 2n) \times (5 + 2n)$ matrix \mathbf{C}^{-1} mentioned in (3.30) can be split into a matrix $\mathbf{C}_{r\phi}^{-1}$ of dimension $(3 + n) \times (3 + n)$ and a matrix \mathbf{C}_{rz}^{-1} of dimension $(2 + n) \times (2 + n)$. From equation (3.30) it follows that for two detector planes, \mathbf{C}_{rz}^{-1} is given by:¹

$$\mathbf{C}_{rz}^{-1} = \begin{pmatrix} 1 & 0 \\ r_1 & 0 \\ 0 & 1 \\ 0 & 0 \end{pmatrix} \begin{pmatrix} w_1^2 & 0 \\ 0 & \lambda_1^2 p_T^2 \end{pmatrix} \begin{pmatrix} 1 & r_1 & 0 & 0 \\ 0 & 0 & 1 & 0 \end{pmatrix} + \begin{pmatrix} 1 & 0 \\ r_2 & 0 \\ r_2 - r_1 & 0 \\ 0 & 1 \end{pmatrix} \begin{pmatrix} w_2^2 & 0 \\ 0 & \lambda_2^2 p_T^2 \end{pmatrix} \begin{pmatrix} 1 & r_2 & r_2 - r_1 & 0 \\ 0 & 0 & 0 & 1 \end{pmatrix} \quad (\text{A.3})$$

with $w_i = 1/\sigma_{i,z}$, and $\lambda_i = k_{i,2}^{-2}$, see equation (3.24). Performing the matrix multiplication gives:

$$\mathbf{C}_{rz}^{-1} = \begin{pmatrix} w_1^2 + w_2^2 & w_1^2 r_1 + w_2^2 r_2 & w_2^2 (r_2 - r_1) & 0 \\ w_1^2 r_1 + w_2^2 r_2 & w_1^2 r_1^2 + w_2^2 r_2^2 & w_2^2 r_2 (r_2 - r_1) & 0 \\ w_2^2 (r_2 - r_1) & w_2^2 r_2 (r_2 - r_1) & w_2^2 (r_2 - r_1)^2 + \lambda_1^2 p_T^2 & 0 \\ 0 & 0 & 0 & \lambda_2^2 p_T^2 \end{pmatrix} \quad (\text{A.4})$$

The determinant of this matrix is given by:

$$\det \mathbf{C}_{rz}^{-1} = \lambda_1^2 p_T^2 w_1^2 \lambda_2^2 p_T^2 w_2^2 (r_2 - r_1)^2 \quad (\text{A.5})$$

From equation (A.2), it follows:

$$\text{cov}(z_0) = C_{rz,11} = \frac{\begin{vmatrix} w_1^2 r_1^2 + w_2^2 r_2^2 & w_2^2 r_2 (r_2 - r_1) \\ w_2^2 r_2 (r_2 - r_1) & w_2^2 (r_2 - r_1)^2 + \lambda_1^2 p_T^2 \end{vmatrix}}{\lambda_1^2 p_T^2 w_1^2 w_2^2 (r_2 - r_1)^2} \quad (\text{A.6})$$

¹ To calculate \mathbf{C}_{rz}^{-1} , also the vectors \mathbf{p} and \mathbf{p}_{ms} and the matrices \mathbf{V}_i and \mathbf{D}_i need to be split into two uncorrelated parts; one in the (r, ϕ) plane and another in the (r, z) plane.

After some manipulation one finally gets:

$$\text{cov}(z_0) = \frac{r_1^2}{\lambda_1^2 p_T^2} + \frac{\frac{r_1^2}{w_2^2} + \frac{r_2^2}{w_1^2}}{(r_2 - r_1)^2} = \frac{k_{1,2}^2 r_1^2}{p_T^2} + \frac{r_1^2 \sigma_{2,z}^2 + r_2^2 \sigma_{1,z}^2}{(r_2 - r_1)^2} \quad (\text{A.7})$$

One can deduce a similar expression for $\text{cov}(a_0)$. The Q/p_T term in equation (3.7) should be ignored in this case, because Q/p_T can not be measured with only two planes.

Appendix B The track equations

In this appendix, the helix trajectory as function of the radius r and track parameters \mathbf{p} is deduced from the equations of motion as function of the time t , magnetic field B_z and particle properties.

The track of a charged particle in a homogenous magnetic field in the positive z -direction is a helix that can be parameterised in the following way:

$$\begin{aligned} x(t) &= x_0 + \rho \cos(Q\omega t - \lambda_0) = x_0 + \rho \cos(Q\lambda - \lambda_0) \\ y(t) &= y_0 - \rho \sin(Q\omega t - \lambda_0) = y_0 - \rho \sin(Q\lambda - \lambda_0) \\ z(t) &= z_0 + v_z t = z_0 + v_T t \cot \theta = z_0 + \rho \lambda \cot \theta \end{aligned} \quad (\text{B.8})$$

with the angular velocity $\omega = v_T/\rho$, the phase $\lambda = \omega t$, and $v_z/v_T = p_z/p_T = \cot \theta$. The term λ_0 is an arbitrary phase that will be obtained by choosing the right start conditions. The terms x_0 and y_0 give the centre of the helix (Figure B.1). The term Q [e] gives the charge of the particle, $Q = +1$ for positrons and $Q = -1$ for electrons. The absolute radius of curvature ρ is given by:

$$\rho[m] = |R_{curv}| = \frac{p_T[\text{GeV}]}{0.3B[\text{T}]} \quad (\text{B.9})$$

The starting time $t = 0$ agrees with the point of minimum distance to the beam axis. The z -position at this point is given by z_0 :

$$z(t = 0) = z_0 \Leftrightarrow \lambda = 0 \quad (\text{B.10})$$

The impact parameter a_0 is given by (Figure B.1):

$$a_0 = Q \left(\sqrt{x_0^2 + y_0^2} - \rho \right) = Q(r_0 - \rho) \Leftrightarrow a_0^2 = r_0^2 + \rho^2 - 2\rho r_0 \quad (\text{B.11})$$

with $r_0 = x_0 \oplus y_0$. It is important to notice the difference between r_0 and $r(0)$. The relation between x_0 , y_0 and ϕ_0 is given by:

$$\begin{aligned} x_0 &= r_0 \cos(\phi_0 - 1/2 Q\pi) = Q r_0 \sin \phi_0 \\ y_0 &= r_0 \sin(\phi_0 - 1/2 Q\pi) = -Q r_0 \cos \phi_0 \end{aligned} \quad (\text{B.12})$$

From (B.8) and (B.12), it follows:

$$\begin{aligned} a_0^2 &= x(0)^2 + y(0)^2 = x_0^2 + y_0^2 + \rho^2 + 2x_0\rho \cos \lambda_0 + 2y_0\rho \sin \lambda_0 \\ &= r_0^2 + \rho^2 + 2\rho Q r_0 \sin(\phi_0 - \lambda_0) \end{aligned} \quad (\text{B.13})$$

Combining (B.11) and (B.13) gives:

$$\lambda_0 = 1/2 Q\pi + \phi_0 \quad (\text{B.14})$$

Equation (B.8) can now be rewritten to:

$$\begin{aligned} x(\lambda) &= x_0 + Q\rho \sin(Q\lambda - \phi_0) \\ y(\lambda) &= y_0 + Q\rho \cos(Q\lambda - \phi_0) \\ z(\lambda) &= z_0 + \rho \lambda \cot \theta \end{aligned} \quad (\text{B.15})$$

From figure B1, it follows:

$$-Qr \sin(\phi - \phi_0) + \rho \cos(\lambda) = r_0 \quad (\text{B.16})$$

with ϕ the angle between the track and the x -axis and ϕ_0 the angle between the track direction and the x -axis at the point of closest approach to the beam-axis. From (B.15), with (B.11) and (B.12), it follows:

$$x^2 + y^2 = r^2 = a_0^2 + 2\rho r_0(1 - \cos(\lambda)) \Rightarrow \cos(\lambda) = 1 - \frac{r^2 - a_0^2}{2\rho r_0} \quad (\text{B.17})$$

Putting (B.17) in (B.16) and using (B.11), gives:

$$r \sin(\phi - \phi_0) = -a_0 - \frac{r^2 - a_0^2}{2Q\rho + 2a_0} \quad (\text{B.18})$$

From this follows:

$$\phi = \phi_0 - \arcsin\left(\frac{a_0}{r} + \frac{r^2 - a_0^2}{2Q\rho r + 2a_0 r}\right) \quad (\text{B.19})$$

For $\rho \gg r \gg a_0$:

$$\phi(r) = \phi_0 - \frac{a_0}{r} - \frac{r}{2Q\rho} \quad (\text{B.20})$$

From equation (B.17) it follows using $\cos(2x) = 1 - 2\sin^2(x)$:

$$2\sin^2(\frac{1}{2}\lambda) = \frac{r^2 - a_0^2}{2\rho r_0} \Leftrightarrow \lambda = 2\arcsin\left(\sqrt{\frac{r^2 - a_0^2}{4\rho^2 + 4Q\rho a_0}}\right) \quad (\text{B.21})$$

Putting this in (B.15) gives:

$$z = z_0 + 2\rho \cot\theta \arcsin\left(\sqrt{\frac{r^2 - a_0^2}{4\rho^2 + 4Q\rho a_0}}\right) \quad (\text{B.22})$$

Or for $\rho \gg r \gg a_0$:

$$z(r) = z_0 + r \cot\theta \quad (\text{B.23})$$

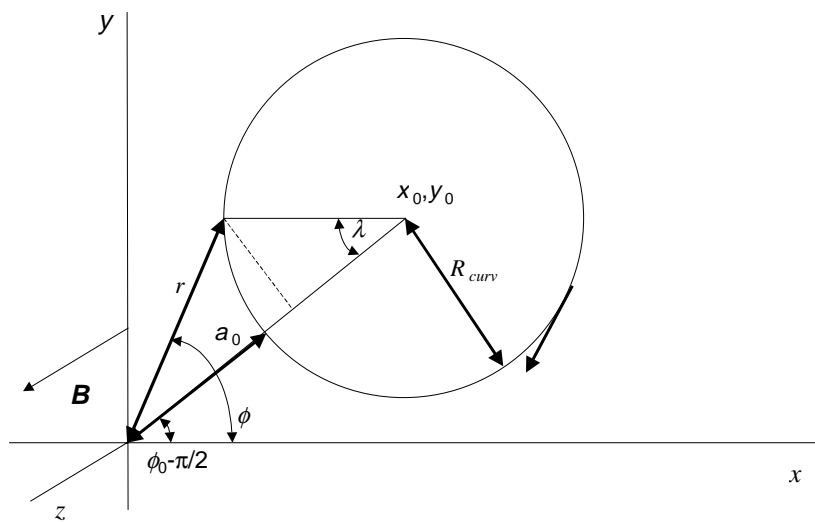


Figure B.1 The track of a particle with positive charge. The true production vertex of the particle can be anywhere on the circle.

Appendix C Calculation of the helix parameters

The five track parameters ($a_0, z_0, \phi_0, \cot\theta, Q/p_T$) can be calculated from the momentum $\vec{p} = (p_x, p_y, p_z)$ of the particle and position $\vec{x}_v = (x_v, y_v, z_v)$ of the production vertex. One should note that knowledge of the track parameters does not allow \vec{p} and \vec{x}_v to be completely reconstructed. The inverse transverse momentum is given by:

$$\boxed{\frac{Q}{p_T} = \frac{Q}{\sqrt{p_x^2 + p_y^2}}} \quad (\text{C.24})$$

The term $\cot\theta$ is given by:

$$\boxed{\cot\theta = \frac{p_z}{p_T}} \quad (\text{C.25})$$

The direction of the particle at the vertex position is given by:

$$\cos\alpha = \frac{p_x}{p_T} \quad \sin\alpha = \frac{p_y}{p_T} \quad (\text{C.26})$$

The co-ordinates of the centre of the helix are given by (B.12) using (B.11):

$$\begin{aligned} x_0 &= x_v + Q\rho \cos(\alpha - 1/2Q\pi) = x_v + Q\rho \sin\alpha \\ y_0 &= y_v + Q\rho \sin(\alpha - 1/2Q\pi) = y_v - Q\rho \cos\alpha \end{aligned} \quad (\text{C.27})$$

The transverse impact parameter a_0 is now given by (B.11):

$$\boxed{a_0 = Q \left(\sqrt{x_0^2 + y_0^2} - \rho \right)} \quad (\text{C.28})$$

The term $\phi_0 [-\pi, \pi]$ is given by:

$$\boxed{\phi_0 = \arctan\left(\frac{y_0}{x_0}\right) + 1/2Q\pi} \quad (\text{C.29})$$

In the case of $|x_0| \ll |y_0|$, it is for numerical reasons better to use:

$$\boxed{\phi_0 = \arctan\left(\frac{p_y}{p_x}\right)} \quad (\text{C.30})$$

The transverse impact parameter z_0 can be calculated using (B.22):

$$\boxed{z_0 = z_v - 2\rho \cot\theta \arcsin\left(\frac{\sqrt{x_v^2 + y_v^2 - a_0^2}}{\sqrt{4\rho^2 + 4Qa_0\rho}}\right)} \quad (\text{C.31})$$

Appendix D Loop corrections, renormalisation and fine-tuning

D.1 Feynman calculus

Important physical quantities in particle physics are cross-sections and decay rates. The calculation of these quantities is based on the **Feynman calculus**. A physical process can schematically be presented with a **Feynman diagram**, the corresponding amplitude can be calculated with the **Feynman rules**. The coupling constants, specifying the strength of the interactions between the particles, the masses of the particles and the four-momenta (E, \mathbf{p}) of these particles determine the amplitude of a process.

D.2 Feynman diagram of loop corrections

Higher order processes cause corrections to be added to the amplitude of a process. Loop corrections are higher order processes where one of the interacting particles temporarily splits off in a particle-antiparticle pair (Figure D.1). In general the contribution to the amplitude of these loop corrections are infinite.



Figure D.1 A lowest order process together with a loop correction.

D.3 Renormalisation

Introducing a cut-off energy Λ up to which the calculation is performed can solve the problem of infinite contributions. The amplitude can now be split off in a finite term, independent of Λ and a divergent term, dependent on Λ . The theory is called **renormalisable** if all divergent Λ dependent terms appear in the form of additions to the masses and coupling constants. This means that the physical (observed) masses and couplings are not the masses and couplings that appeared in the original Feynman rules but renormalised ones:

$$m_{\text{physical}} = m + \delta m \quad g_{\text{physical}} = g + \delta g \quad (\text{D.1})$$

Only m_{physical} and g_{physical} are measured. Compensating infinities in the bare mass m and coupling g cancel the infinite terms δm and δg (for $\Lambda \rightarrow \infty$). For each chosen value of the cut-off energy Λ , a corresponding value of m and g can be calculated which matches with m_{physical} and g_{physical} .

The **naturalness** of a system describes how much the values of m and g depend on the cut-off energy Λ . In a natural system δm scales with $\log \Lambda$. This means that the corrections are small until the GUT scale:

$$\frac{\delta m(\Lambda = 10^{15} \text{ GeV})}{m_{\text{physical}}} \ll 1 \quad (\text{D.2})$$

Fine-tuning is necessary if δm depends strongly on Λ , e.g. δm scales with Λ^2 . In this case m (and g) depend strongly on the chosen value for the cut-off energy and the order up to which the loop corrections are included:

$$\frac{\delta m(\Lambda = 10^{15} \text{ GeV})}{m_{\text{physical}}} \gg 1 \quad (\text{D.3})$$

From the theoretical viewpoint fine-tuning is not an elegant solution.

D.4 Running masses and couplings

The loop diagrams give also rise to finite (Λ independent) contributions to the amplitude. These contributions lead to modifications in m and g , which are functions of the energy of the particles involved. This means that the effective (observed) masses and coupling constants depend on the energies of the particles involved (**running masses and running coupling constants**). This dependence is described by the so-called **renormalisation group equations** and is typically rather small at low energies, $O(1 \text{ TeV})$, and can usually be ignored. The evolution has however important consequences at high energies, $O(10^{15} \text{ GeV})$, and is the basic idea behind the grand unification model.

Appendix E Calculation of space-points

E.1 Introduction

This appendix derives the axial position L'_2 (in the co-ordinate frame of the module on the “ ϕ -layer”) of the crossing point of a cluster on the “ ϕ -layer” with transversal position T and a cluster on the “stereo-layer” with transversal position T' . The barrel part is described in section E.2. The end-cap part is described in section E.3.

E.2 Barrel SCT

The terms (T_2, L_2) give the local co-ordinates of a point on the “stereo-layer”. A rotation with angle $-\alpha$ gives the position in the co-ordinate frame of the module on the “ ϕ -layer” (T'_2, L'_2) :

$$\begin{aligned} T'_2 &= T_2 \cos \alpha - L_2 \sin \alpha \\ L'_2 &= L_2 \cos \alpha + T_2 \sin \alpha \end{aligned} \quad (\text{E.1})$$

T'_2 as function of L'_2 is given by:

$$T'_2 = \frac{T_2 - L'_2 \sin \alpha}{\cos \alpha} \quad (\text{E.2})$$

On the crossing point:

$$T'_2 = T_1 \quad (\text{E.3})$$

From this follows:

$$L'_2 = L_1 = \frac{T_2 - T_1 \cos \alpha}{\sin \alpha} \quad (\text{E.4})$$

E.3 End-cap SCT

In the end-cap part the detector modules have a wafer structure. A consequence of this is that the strips are not placed parallel (like in the barrel). Each space-point can be expressed in two different local co-ordinate frames. A cylindrical frame $(P(\text{cm}), \Phi(\text{mrad}))$ with axes parallel and perpendicular to each strip, and a Cartesian frame $(L(\text{cm}), T(\text{cm}))$ with axes parallel and perpendicular to the most central strip only. In both frames $(0, 0)$ corresponds with the centre of the module. The conversion from the first frame to the second is given by (figure E.1):

$$\begin{aligned} L &= (P + r_{mod}) \cos \Phi - r_{mod} \\ T &= (P + r_{mod}) \sin \Phi \end{aligned} \quad (\text{E.5})$$

The terms (L_1, T_1) give the local position of a cluster on the “ ϕ -layer”; the terms (L_2, T_2) give the local position of a cluster on the “stereo-layer”. A transformation is necessary to express (L_2, T_2) in the co-ordinate frame of the module on the “ ϕ -layer”:

$$\begin{aligned} L'_2 &= L_2 \cos \alpha - T_2 \sin \alpha \\ T'_2 &= T_2 \cos \alpha + L_2 \sin \alpha \end{aligned} \quad (\text{E.6})$$

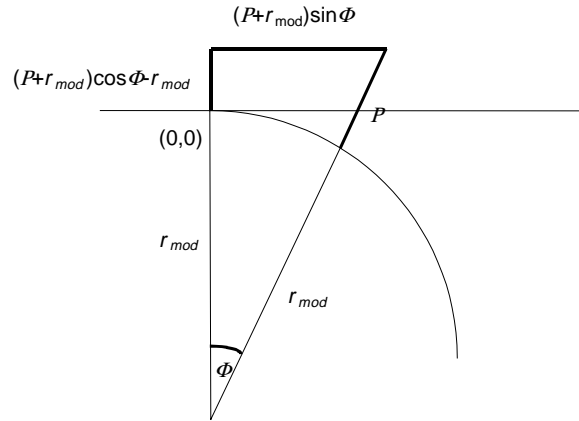


Figure E.1 Conversion from local cylindrical to local Cartesian co-ordinates.

with α the rotation angle of the module. Combining (E.5) and (E.6) gives:

$$\begin{aligned} L'_2 &= -r_{mod} \cos \alpha + P_2 \cos \alpha \cos \Phi_2 - P_2 \sin \alpha \sin \Phi_2 + \\ &\quad r_{mod} \cos \Phi_2 \cos \alpha - r_{mod} \sin \Phi_2 \sin \alpha \\ T'_2 &= P_2 \sin \Phi_2 \cos \alpha - r_{mod} \sin \alpha + P_2 \sin \alpha \cos \Phi_2 + \\ &\quad r_{mod} \cos \Phi_2 \sin \alpha + r_{mod} \sin \Phi_2 \cos \alpha \end{aligned} \quad (E.7)$$

One the point where the cluster on the “ ϕ -layer” and the “stereo-layer” cross each other:

$$\begin{aligned} L_1 &= L'_2 \\ T_1 &= T'_2 \end{aligned} \quad (E.8)$$

Combining (E.7) with (E.8) gives:

$$\begin{aligned} -r_{mod} + F_1 \cos \Phi_1 + r_{mod} \cos \Phi_1 &= -r_{mod} \cos \alpha + \\ &\quad P_2 \cos \alpha \cos \Phi_2 - P_2 \sin \alpha \sin \Phi_2 + r_{mod} \cos \Phi_2 \cos \alpha - r_{mod} \sin \Phi_2 \sin \alpha \\ P_1 \sin \Phi_1 + r_{mod} \sin \Phi_1 &= P_2 \sin \Phi_2 \cos \alpha - \\ &\quad r_{mod} \sin \alpha + P_2 \sin \alpha \cos \Phi_2 + r_{mod} \cos \Phi_2 \sin \alpha + r_{mod} \sin \Phi_2 \cos \alpha \end{aligned} \quad (E.9)$$

Using the summation rules:

$$\begin{aligned} \cos(x + y) &= \cos x \cos y - \sin x \sin y \\ \sin(x + y) &= \sin x \cos y + \cos x \sin y \end{aligned} \quad (E.10)$$

gives:

$$\begin{aligned} -r_{mod} + F_1 \cos \Phi_1 + r_{mod} \cos \Phi_1 &= -r_{mod} \cos \alpha + F_2 \cos(\alpha + \Phi_2) + r_{mod} \cos(\alpha + \Phi_2) \\ P_1 \sin \Phi_1 + r_{mod} \sin \Phi_1 &= -r_{mod} \sin \alpha + P_2 \sin(\alpha + \Phi_2) + r_{mod} \sin(\alpha + \Phi_2) \end{aligned} \quad (E.11)$$

After some manipulation one gets:

$$P_1 = r_{mod} \frac{\sin \Phi_2 - \sin(\Phi_2 + \alpha)}{\sin(\Phi_1 - (\Phi_2 + \alpha))} - r_{mod} \quad (E.12)$$

Glossary

Between brackets is given the context in which the term is used.

A \oplus B-model (inner detector)	Simple model describing the resolution and correlations of the helix parameters as function of the transverse momentum p_T , see also chapter 3.
Absorption length	The absorption length is the length in which a highly energetic hadron loses all but a fraction $1/e$ of its energy on average.
Architecture A (LVL2)	A possible architecture for the LVL2 system with the FEX processors based on FPGA technology, see also chapter 5.
Architecture B (LVL2)	A possible architecture for the LVL2 system with the local and global part implemented on two separate processor farms. The ROB's push their data to the FEX processors, see also chapter 5.
Architecture C (LVL2)	A possible architecture for the LVL2 system with the local and global part implemented on one big processor farm. The LVL2 processors pull the data from the ROB's, see also chapter 5.
Architecture C' (LVL2)	Combination of architecture C and A with the FPGA processors used as a kind of co-processors for specific time consuming tasks, see also chapter 5.
assert macro (C/C++ programming)	Standard ANSI C macro. If NDEBUG is not defined, the macro is expanded in the C pre-processing step to a routine, which stops the program with an error message if the passed argument is false. Expanded to nothing if NDEBUG is defined.
ATLAS	ATLAS (A Toroidal LHC ApparatuS) is one of the four future LHC experiments, see also chapter 2.
ATLFAST/ATLFAST++	The FORTRAN package ATLFAST provides a fast simulation of the ATLAS detector based on parameterisation. See also chapter 3 and chapter 4. The program ATLFAST++ is a C++ version of ATLFAST.
ATM	ATM (A synchronous Transfer Mode) is a technology for switch components, developed by telecommunication industry.
ATRIG	The FORTRAN package ATRIG is developed for the study of the physics performance of the LVL1 and LVL2 trigger system and the production of data samples of events that passed LVL1 and eventually LVL2. This package is not suited for studying the execution time of the algorithms.
Barrel (ATLAS)	The part of the ATLAS detector for $ \eta \leq 1.4$ (approximately, dependent on the sub-detector). The inner detector layers are positioned on cylindrical surfaces around the beam axis.
Beam constraint (inner detector)	A constraint that a track is created at (or very close to) the primary vertex. This constraint can be used as extra measurement of the transverse position with value zero and standard deviation equal to the beam radius.
Benchmark (C/C++ programming)	A measurement of the calculation time of an algorithm.
B-layer (precision tracker)	First barrel pixel layer of ATLAS detector, especially useful for B-physics studies.

Bremsstrahlung	Bremsstrahlung is the production of photons by a highly energetic electron giving rise to energy losses of the electron.
Bunch (LHC)	A bunch is a packet of accelerated protons at LHC. In a bunch-crossing two bunches are colliding, generally causing one or several events (mostly of the minimum bias type).
Central solenoid (ATLAS)	The central solenoid generates the solenoidal magnetic field in which the inner detector is placed.
Centre-of-mass energy	The centre-of-mass energy of a collision of two particles of energy E_1 and E_2 and momentum \mathbf{p}_1 and \mathbf{p}_2 is given by: $E_{cm} = \sqrt{(E_1 + E_2)^2 - (\mathbf{p}_1 + \mathbf{p}_2)^2}$
Chargino (SUSY)	The charginos (\tilde{X}_i^\pm) are a group of charged spin $\frac{1}{2}$ particles, predicted in the MSSM, see also chapter 4.
Class (C++ programming)	A class is an aggregate of named data elements, possibly of different types, and a set of operations, designed to manipulate that data.
Cluster (ATLAS)	A cluster is an adjacent group of pixels or SCT strips with a hit or a group of calorimeter cells with an energy deposited above threshold.
Coil rib (muon spectrometer)	Coil ribs are radial reinforcements of the barrel coils of the muon spectrometer.
Common block (FORTRAN programming)	A common block is an area of storage in a FORTRAN program. The data stored in a common block can be accessed by all routines.
CPU	C entral P rocessor U nit
CSC (muon spectrometer)	CSC (Cathode Strip Chamber) is a type of detector used in the ATLAS muon spectrometer, see also chapter 2.
DAQ (ATLAS)	The ATLAS DAQ (Data Acquisition) system controls the permanent storage of data from events accepted by the ATLAS trigger system and the data generated within the trigger system.
Data driven system (LVL2)	LVL2 system based on FPGA technology, see also chapter 5.
Data rate	The data rate [KB/s] is the amount of data passing per second. Follows from the event rate and the data size per event.
Detector simulation	Simulation of the response of the (ATLAS) detector on particles passing through it. Full detector simulation is simulation based on GEANT and DICE. Fast detector simulation is simulation based on parameterisation (ATLFAST).
DICE (ATLAS)	The FORTRAN package DICE (Detector Integration Code) provides a detector geometry description of the ATLAS detector and an interface to GEANT. The simulation of the electronic response of the detector to particles is also provided by DICE.
DMA	DMA (Direct Memory Access) is the transfer of data in a processor independent from the main CPU.
Drift tube/drift chamber	Detector technique used in particle physics experiments with wires on a high voltage strung parallel in a gas volume, closed by conducting planes on a low voltage. A charged particle crossing this gas volume may be detected by the ionisation trail it leaves behind in the gas.
DS	DS is a protocol for high-speed data communication links.

End-cap (ATLAS)	The part of the ATLAS detector for $ \eta > 1.4$ (approximately, dependent on the sub-detector). The inner detector layers are mounted on discs around the beam pipe.
Event (LHC)	An event is an interaction between beam particles at LHC, giving rise to a signal in the detector.
Event builder (DAQ)	The event builder is the part of the DAQ system collecting the information from all parts of all sub-detectors, for a given bunch-crossing, see also chapter 5.
Event filter (ATLAS)	The ATLAS third level trigger system, called LVL3 in the past, see also chapter 5.
Event generator	Monte Carlo computer program used for the simulation of events.
Event rate	The event rate [Hz] is the number of accepted events per second.
FAST OR (pixel detector)	A FAST OR is a readout option for the pixel detector, especially developed for trigger purposes, where the pixels are summed along one row or column. The pixel detector behaves like a kind of strip detector in this case.
Features (LVL2)	Parameters of the reconstructed track calculated by the LVL2 FEX algorithm, e.g. η , p_T , E_T and ϕ .
FEX (LVL2)	FEX (Feature EXtraction) is the reconstruction of tracks and clusters in the LVL2 system. Only RoI data is used.
Finite element method	Simulation method for the calculation of the dynamics of a large complicated object. The object is split in a finite number of small objects for which the dynamics can be described. In general used for the calculation of mechanical structures, temperature distributions and magnetic field distributions.
Forward (ATLAS)	The end-cap part of the detector at positive z . The opposite side is called backward part. For the calorimeter the term forward is also used for the part extending from $\eta = 3.1$ to $\eta = 4.9$.
FPGA processor (LVL2)	An FPGA (Field Programmable Gate Array) processor is a LVL2 processor based on dedicated hardware and running in a pipelined fashion, see also chapter 5.
Fragmentation (SM)	Fragmentation describes together with hadronisation the formation of hadrons from individual quarks. A quark q_0 can split of a $q_1\bar{q}_1$ pair (fragmentation), such that a meson $q_0\bar{q}_1$ can be formed (hadronisation), with a q_1 left behind. This q_1 can at a later stage pair off with a \bar{q}_2 and so on.
Front-end electronics (ATLAS)	Electronics for the readout of the ATLAS detector, partially placed on the detector itself, partially placed close to the detector. The front-end electronics is partially integrated with the LVL1 system.
GEANT	GEANT is a FORTRAN package for the tracking of stable particles through the (ATLAS) detector. The influence of magnetic fields, ionisation energy loss, multiple scattering, bremsstrahlung, photon conversions, nuclear interactions of hadrons and the decay of long-lived particles are taken into account.

Global co-ordinate (LVL2 pre-processing)	Co-ordinate defined in the co-ordinate frame of the ATLAS detector.
Global part (LVL2)	The second part of the LVL2 algorithm. The features for the different sub-detectors calculated in the local part are combined into a final LVL2 acceptance/rejection decision.
Gluino (SUSY)	The gluinos (\tilde{g}) are the spin $\frac{1}{2}$ partners of the gluons, predicted in the MSSM, see also chapter 4.
Gold-plated decay (LHC)	The decay of the Higgs boson into four charged leptons.
GTP (LVL2)	A GTP (Global Trigger Processor) performs the global part of the LVL2 algorithm, see also chapter 5.
GUT	GUT (Grand Unification Theory) models are based on the assumption that the strong, weak and electromagnetic forces in nature unify at an ultra high energy of order 10^{15} GeV, see also chapter 1 and chapter 4.
Hadronisation (SM)	See fragmentation.
Helix parameters (inner detector)	Parameters describing a track in the solenoid magnetic field of the inner detector, see also chapter 3.
Higgs boson (SM)	The Higgs boson (H^0) is a neutral spin 0 particle predicted in the SM. In the MSSM additional Higgs bosons are occurring (h^0, A^0, H^\pm), see also chapter 1 and 4.
Hit (precision tracker)	A strip or pixel in the precision tracker with a signal.
Inefficiency (precision tracker)	The probability that the passage of a charged particle through a detector element of the precision tracker does not cause a hit.
Inline function (C/C++ programming)	A (small) C/C++ function with each call to it replaced by the expansion of its body, preventing the overhead of a function call. Inline functions are used to speed up programs.
Inner detector (ATLAS)	The precision tracker combined with the TRT.
Interface (C/C++ programming)	Protocol describing the number and types of variables to be passed to a subroutine or function and the type of the returned value.
Interrupt (computing)	A computer interrupt is a (temporary) interrupt of the task currently being performed on a computer system by a task with a higher priority.
Intrinsic (detector) resolution (inner detector)	Measurement resolution for an ideal track (bremsstrahlung and multiple scattering are not taken into account). For the precision tracker mainly determined by the pitch of the microstrips and pixels.
Invariant mass	The invariant mass of a particle is given by $E^2 - \mathbf{p}^2$, with E the particle energy and $\mathbf{p} = (p_x, p_y, p_z)$ the particle momentum. This quantity is independent of the used reference frame.
ISAJET	ISAJET is a commonly used event generator, also for SUSY events, written in FORTRAN. See also chapter 4.
Jet (SM)	A jet is a stream of several particles in the same direction, created by a quark or gluon with a large kinetic energy. Jets contain hadrons like pions and kaons, but through further decays they may include muons, photons and electrons as well.
Latency (LVL1/LVL2)	Time necessary to calculate and distribute a trigger decision at LVL1 or LVL2.

LEP	LEP (L arge E lectron P ositron collider) is an electron-positron collider at CERN with 174 GeV centre-of-mass energy (1996).
Leptoquarks	Leptoquarks are particles predicted in some models extending the SM carrying both lepton and baryon quantum numbers.
LHC	LHC (L arge H adron C ollider) is a new 14 TeV centre-of-mass energy proton-proton collider to be built at CERN.
Local co-ordinate (LVL2 pre-processing)	Co-ordinate defined in the co-ordinate frame of a detector module of the precision tracker. Position (0, 0) is equal to the centre of the module, see also chapter 6.
Local part (LVL2)	The first part of the LVL2 algorithm. This part consists of feature extraction for the different sub-detectors, see also chapter 5.
Longitudinal impact parameter (inner detector)	The longitudinal impact parameter (z_0) is one of the helix parameters, describing the position along the beam axis where the transverse impact parameter a_0 is evaluated.
LSP (SUSY)	Lightest sparticle, stable and neutral in the MSSM, see also chapter 4.
Luminosity	The luminosity [$\text{cm}^{-2}\text{s}^{-1}$] is a quantity describing the performance of a collider experiment, see also chapter 1. The number of events collected over a given period of time can be calculated from the product of the production cross-section and the luminosity. LHC will reach a luminosity of $L_{design} = 10^{34} \text{ cm}^{-2}\text{s}^{-1}$ (high luminosity). The first few years of operation LHC will run at a lower luminosity of $L_{initial} = 10^{33} \text{ cm}^{-2}\text{s}^{-1}$.
LUT (C/C++ programming)	A LUT (L ook U p T able) is a table containing pre-calculated results of a (mathematical) function or algorithm. The use of LUTs can speed up algorithms.
LVL1 (ATLAS)	The ATLAS first level trigger system, see also chapter 5.
LVL2 (ATLAS)	The ATLAS second level trigger system, see chapter 5.
Macro (C/C++ programming)	A set of C/C++ statements with an interface. In the C/C++ pre-processor each call to the macro is replaced by an expansion of the macro body. A macro is in principle similar but more primitive than an inline function.
Majorana fermion	Fermion being a particle and antiparticle at the same time.
MAPPER	The C++ program MAPPER is developed for studying ROB-RoI relations for the inner detector, e.g. the mean number of SCT ROBs receiving an RoI request. See also chapter 5.
Massive vector bosons (SM)	The massive vector bosons (Z^0 , W^+ , W^-) are a group of fundamental spin 1 particles in the SM mediating the weak force, see also chapter 1.
MDT (muon spectrometer)	MDT (pressured M onitored D rift T ube) is a type of detector used in the ATLAS muon spectrometer, see chapter 2.
Minimum bias event (LHC)	A soft collision between two partons at LHC, causing a background signal. Each hard interaction at LHC will be accompanied by about 25 minimum bias events.

Missing transverse energy/momentum	Transverse energy/momentum carried by particles that are not detected due to detector limitations or that can not be detected (neutrinos, SUSY LSP).
Module (precision tracker)	A module is the smallest detector unit (substrate) except from an individual strip or pixel. A SCT module consists of 768 microstrips. A pixel module consists of 614440 pixels.
Monte Carlo program	Simulation program based on a random number generator.
MSSM	The MSSM (M inimal S upersymmetric S tandard M odel) is the simplest supersymmetric extension of the standard model, see also chapter 4.
Multiple (Coulomb) scattering	A charged particle traversing a medium is deflected by many small-angle scatters. Most of this deflection is due to Coulomb scattering from nuclei, and hence the effect is called multiple Coulomb scattering.
Neutralino (SUSY)	The neutralinos (\tilde{X}_i^0) are a group of neutral spin 0 particles, predicted in the MSSM, see also chapter 4. The lightest neutralino \tilde{X}_1^0 is the LSP in most SUSY models.
NIM	NIM specifies logical levels and crates for modules with logical switches.
Online/Offline selection	Online selection algorithms run in real time, e.g. at LVL2. Offline selection algorithms run on the permanently stored data that passed the online selection. Offline algorithms are much less time critical than online algorithms.
Particle identification efficiency	The efficiency (of a detector and reconstruction algorithm) to distinguish particles of different type, e.g. how well electrons can be distinguished from muons.
Parton	A fundamental particle (no bound state), can be a lepton, quark or force carrying boson.
Parton distribution function	Function $f(x, y, E)$ describing the probability that a fraction x ($0 \leq x \leq 1$) of the total particle energy E is carried by a parton y .
Pattern recognition (inner detector)	Track reconstruction in the inner detector. The assignment of wrong hits to the reconstructed track is referred to as pattern recognition errors.
PDFLIB	Numerical library containing several parton distribution functions.
PDG	The PDG (P article D ata G roup) publishes the <i>Review of Particle Properties</i> , containing information about the properties of elementary particles and their interactions.
Physics performance (LVL2 FEX)	The physics performance of a LVL2 FEX algorithm is the efficiency of the algorithm for accepting signal events together with the efficiency for rejecting background events.
File up (LHC)	Minimum bias events superimposed on an interesting event.
Pixel detector (ATLAS)	Semiconductor tracking detector based on silicon pixel technology. The pixel detector consists of three barrel layers and three end-cap disks on both sides, see also chapter 2.

Pointer (C/C++ programming)	A variable with as contents the memory address of another variable.
Polar angle (LHC)	The polar angle (θ) is given by: $\cot\theta = r/z$, with r the distance from the beam axis and z the position along the beam axis.
Precision tracker (ATLAS)	The SCT combined with the pixel detector.
Pre-processing (LVL2)	Selection of hits to be used in the LVL2 FEX algorithm and combination/transformation of the hits into a format suitable for the FEX algorithm, see also chapter 6.
Pre-processor (C/C++ programming)	The C/C++ pre-processor is a processing step before the actual compilation. Depending on the used pre-processor definitions, the C/C++ code to be compiled is selected, macros are expanded to normal C/C++ statements and header files, containing C/C++ definitions, are included.
PRESOL	Monte Carlo computer simulation program of the ATLAS detector, written in FORTRAN, calculating for a track with a given pair of p_T and η values the corresponding covariance matrix of the helix parameters. Both the intrinsic detector resolution and multiple scattering are taken into account. See also chapter 3.
Processor farm (LVL2)	A farm of trigger processors, operating in parallel, running the local and/or global part of the LVL2 algorithm, see also chapter 5.
Proportional chamber	Drift chamber with a linear dependence between the measured detector signal and the energy of the crossing particle.
PROSPINO	PROSPINO, written in FORTRAN, is a Monte Carlo simulation program for the calculation of the production cross section of squarks and gluinos at hadron colliders, see also chapter 4.
PSD (C/C++ programming)	Program Structure Diagram
Pseudorapidity	The pseudorapidity (η) is given by: $\eta = -\ln(\tan\theta/2)$, with θ the polar angle.
Pull architecture (LVL2)	Architecture option for the LVL2 system. The FEX processors request their data from the ROBs in this case, see also chapter 5.
Push architecture (LVL2)	Architecture option for the LVL2 system. The ROBs push their data to the FEX processors in this case, see also chapter 5.
PYTHIA/SPYTHIA	The FORTRAN package PYTHIA is a commonly used event generator. SPYTHIA is an extension of PYTHIA 5.7, necessary for the simulation of SUSY events. See also chapter 4.
Radiation length	The radiation length is the length in which a highly energetic electron loses all but a fraction $1/e$ of its energy to bremsstrahlung on average.
Rapidity	The rapidity (y) is given by: $y = \operatorname{atanh}(p_z/E)$, with p_z the momentum along the beam line and E the particle energy. For massless particles the rapidity is equal to the pseudorapidity.
Raw data (LVL2)	A data fragment in a ROB in the format as received from a ROD, see also chapter 5.
Recursive routine (C/C++ programming)	A routine that can make a call to itself, generally with a different set of parameters.

Reducible/irreducible background	Reducible background produces a signal that is in principle different from the signal produced by the event of interest. Due to experimental restrictions this signal can however be misidentified as a similar signal. Irreducible background produces the same signal as the signal produced by the event of interest.
ROB (LVL2)	A ROB (ReadOut Buffer) is a data buffer keeping the data from the complete ATLAS detector during the LVL2 processing, via the RODs connected to the LVL1 system and via the event builder connected to the event filter, see also chapter 5.
ROD (LVL1)	A ROD (ReadOut Driver) is the most downstream element of the LVL1 system, communicating directly with the ROBs of the LVL2 system, see also chapter 5.
RoI (ATLAS)	An RoI (Region of Interest) is a region limited in η and ϕ , indicated by the LVL1 trigger to contain candidates for objects requiring further analysis at LVL2. In the case of B-physics trigger RoIs can also be defined internally by the LVL2 system (TRT full scan). The RoIs can be divided in primary RoIs and secondary RoIs . A primary RoI contributed to the LVL1 trigger acceptance decision. A secondary RoI did not contribute to the LVL1 acceptance decision, e.g. the energy was too low.
RoI builder (LVL2)	Part of the LVL2 supervisor receiving the RoI information from the LVL1 system. In the RoI builder the RoIs are identified and formatted for LVL2.
RoI fragment (LVL2)	The part of the RoI data residing in a single ROB.
RoI module (LVL2 FEX)	A detector module with a (η, ϕ) range overlapping with the (η, ϕ) range of the RoI.
RoI pointer (LVL2)	An RoI pointer is a pointer to a small region in η and ϕ , indicated by the LVL1 trigger. Based on the RoI pointers the RoIs are created, see also chapter 5.
RoI request (LVL2)	Request for data sent from the LVL2 supervisor or trigger processor to the ROBs involved in the current RoI, see also chapter 5.
RoIC (LVL2)	RoIC (RoI Concentration) is the combination of RoI fragments into full RoIs, see also chapter 5.
R-parity (SUSY)	Quantum number predicted in the MSSM, see also chapter 4. $R = 1$ for SM particles, $R = -1$ for the supersymmetric partners.
RPC (muon spectrometer)	An RPC (Resistive Plate Chamber) is a type of detector used in the trigger system of the ATLAS muon spectrometer, see also chapter 2.
RSI (LVL2)	An RSI (ROB to Switch Interface) is an interface component placed between the ROBs and the LVL2 switch, see also chapter 5.
Scintillator	Type of detector used in particle physics experiments for energy measurements by total absorption. Based on the creation of excited molecules and the detection of the created optical photons.
SCT (ATLAS)	The SCT (SemiConductor Tracker) is a tracking detector based on silicon microstrip technology. The SCT consists of four barrel layers and nine end-cap disks on both sides, see also chapter 2.

SCTFEX	The C++ program SCTFEX contains an implementation of a pre-processing and LVL2 track finding algorithm for the precision tracker. See also chapters 6 and 7.
Services (ATLAS)	Services are auxiliary elements of the ATLAS detector like cables, cooling pipes and support structures.
SFI (LVL2)	An SFI (S witch to F arm I nterface) is an interface component placed between the LVL2 switch and the processor farm, see also chapter 5.
Shower	A shower is the cascade production of secondary particles initiated by a highly energetic particle that was incident on a thick absorber.
Slepton (SUSY)	A slepton (\tilde{l}) is the spin 0 partner of a lepton, predicted in the MSSM, see also chapter 4.
SM	Standard Model of particle physics, describing the elementary particles existing in nature, their properties and their interactions. See also chapter 1.
Space-point (LVL2 FEX)	Global (ϕ, r, z) co-ordinate reconstructed from one or several hits, see also chapter 6.
Sparticle (SUSY)	A sparticle is the supersymmetric partner of a particle with $R = -1$. See also chapter 4.
Squark (SUSY)	A squark (\tilde{q}) is the spin 0 partner of a quark, predicted in the MSSM, see also chapter 4.
Stereo layer/stereo angle (SCT)	The second detection layer of a SCT module. The microstrips make a small stereo angle of 40 mrad with the radial axis, see also chapter 2.
Strut (muon spectrometer)	Struts provide an outer azimuthal connection between the barrel toroid coils of the muon spectrometer.
Sub-detector (ATLAS)	The ATLAS detector is divided in several sub-detectors: SCT, pixel detector, TRT, electromagnetic calorimeter, hadronic calorimeter and muon spectrometer.
SUGRA	The SUGRA model combines the MSSM with supergravity and grand unification. The SUGRA model can be described by five parameters: $m_0, m_{1/2}, \tan\beta, A_0$ and $\text{sign}(\mu)$. See also chapter 4.
Supergravity	A supersymmetric extension of the standard model including the gravitational interaction. The partner of the graviton is called gravitino, see also chapter 4.
Superlayer (PRESOL)	Simplified implementation of the TRT in PRESOL. Several layers of straw tubes are regarded as one superlayer, see also chapter 2.
Supervisor (LVL2)	The part of the LVL2 system that manages the complete LVL2 system, especially the assignment of processors and the distribution of RoI requests and trigger decisions. See also chapter 5.
SUSY	SUSY (S Uper S Ymmetry) is a possible extension of the SM assuming a symmetry between the fermionic and bosonic degrees of freedom. See also chapter 4.
Switch (LVL2)	A switch is an electronic component linking several sources to several destinations.
TDR (ATLAS)	Technical Design Report

TEVATRON	The TEVATRON is a 2 TeV centre-of-mass energy proton-antiproton collider at FermiLab.
TGC (muon spectrometer)	TGC (Thin Gap Chamber) is a detector technology used in the trigger system of the ATLAS muon spectrometer, see also chapter 2.
Tilt angle (precision tracker)	The tilt angle is the angle between the normal of a module and the radial axis.
Toroid (ATLAS)	Magnet generating a toroidal magnetic field in which the muon spectrometer is placed.
TP	Technical Proposal
Track	Trajectory of a charged particle through the magnetic field of a tracking detector.
Tracker	Detector developed for the reconstruction of charged tracks and the determination of the helix parameters.
Transverse energy/momentum	The transverse energy/momentum (E_T, p_T) is the energy/momentum component in the plane perpendicular to the beam axis.
Transverse impact parameter (inner detector)	The transverse impact parameter (a_0) is one of the helix parameters describing the distance of closest approach to the beam-line.
Transverse sphericity	The transverse sphericity (S_T) is the ratio of eigenvalues of the sphericity tensor in transverse plane, see section 4.7.4.
Trigger (ATLAS)	The online selection of events, which need to be stored and analysed further offline.
Trigger menu (LVL1/LVL2)	The trigger menu describes the event selection criteria at LVL1 and LVL2 and consists of trigger menu items. The trigger menu with secondary RoIs is also referred to as extended menu . See also chapter 5.
Trigger menu item (LVL1/LVL2)	A trigger menu item consists of a combination of trigger objects .
Trigger object (LVL1/LVL2)	A trigger object includes the required number of RoIs of each type and the requirements on properties of these RoIs (e.g. p_T threshold).
Trigger processor (LVL2)	A trigger processor is a GTP or FEX processor.
TRT (ATLAS)	The TRT (T ransition R adiation T racker) is a detector based on straw tubes technology, see also chapter 2.
TRT (full) scan (LVL2)	TRT LVL2 track reconstruction not guided by RoIs. This step can be necessary for B-physics.
Vertex	Interaction point. The point of the hard interaction is referred to as primary vertex . The decay point of an unstable particle is referred to as secondary vertex .
Virtual function (C/C++ programming)	A C/C++ function (interface) with several implementations. Which implementation of the virtual function is called is decided at run time.
Virtual particle	A particle that is not on its mass shell
VME	VME (V ersatile M odule E urope) is a computer bus for 32-bits microprocessor systems.
Voussoir (muon spectrometer)	The voussoirs provide an inner azimuthal connection between the barrel toroid coils of the muon spectrometer.

XKALMAN
(inner detector)
 ϕ -layer (SCT)

XKALMAN is an offline track reconstruction algorithm for the inner detector.

The first detection layer of a SCT module with the microstrips placed radially.

Summary

In this thesis I describe a study of the physics performance of the ATLAS inner detector and a study of aspects of the second level trigger for the ATLAS inner detector. In particular I have studied a parameterisation of the track reconstruction performance for muons as function of the pseudorapidity η and transverse momentum p_T and a track reconstruction algorithm for high- p_T charged particles for the second level trigger. Additionally I present results of studies on the response of the ATLAS detector for supersymmetric events and cross-section calculations for the production of supersymmetric events.

In chapter 1 I shortly discuss the standard model of particle physics (SM). I describe the most important properties of the Large Hadron Collider (LHC) at CERN and its physics potential. The LHC is a future 14 TeV proton-proton collider with a design luminosity $L_{design} = 10^{34} \text{ cm}^{-2}\text{s}^{-1}$ and a bunch-crossing frequency of 40 MHz. LHC is planned to start operating in 2005.

The most important physics study at LHC is the search for and measurement of the properties of the Higgs boson in the mass range from about 80 GeV until about 1 TeV. In addition to Higgs physics, the LHC will allow us to study the bottom and top quark in great detail. Possible extensions of the standard model, like supersymmetry (SUSY), can also be tested on their validity.

In chapter 2 I introduce the ATLAS experiment, which is one of the four future LHC experiments. From the collision point outwards, the ATLAS detector is built up from tracking detectors (inner detector), followed by calorimeters and again tracking detectors (muon spectrometer). Tracking detectors measure the position of a crossing charged particle with minimal disturbance. Calorimeters absorb most particles. The energies, positions of incidence and directions of flight of the particles can be measured as a part of the energy deposited is converted into light or charge. The complete inner detector is placed in a solenoid magnet with a central field of 2 T and a bending power of 2.1 Tm. The muon spectrometer is placed in a toroidal magnetic field with a bending power of 3-6 Tm. The complete ATLAS detector is split into a barrel part, where detector layers are positioned on cylindrical surfaces around the beam axis, and two end-cap parts, where detector layers are positioned perpendicular to the beam axis.

In this chapter I shortly describe the ATLAS magnet system, the calorimeter system and the muon spectrometer. I describe the inner detector in more detail. The inner detector is the part of the ATLAS detector placed the closest to the interaction point. It combines high-resolution silicon pixel and silicon microstrip (SCT) detectors on the inside with continuous tracking elements (TRT) on the outside.

In chapter 3 I present a parameterisation of the reconstruction accuracy of the ATLAS inner detector for muon tracks. This parameterisation is used in the software package ATLFAST. For a given set of parameters, describing a muon track in the magnetic field of the inner detector, a smeared set of parameters can be calculated, which approximate the real parameters measured. In the parameterisation the influence of the intrinsic detector resolution, multiple scattering and the correlation between the track parameters is taken into account.

I have calculated the resolutions of the track parameters and their correlations as function of the pseudorapidity η and transverse momentum p_T . I have investigated the influence of different models of the magnetic field in the inner detector, and the influence of the presence and the use of data from the first pixel layer (B-layer) on the performance. Based on this parameterisation, I have studied the performance of the combined inner detector/muon spec-

trometer and the accuracy of the muon charge identification. Finally I shortly describe possible methods for extending the parameterisation to include electrons and pions, to include track reconstruction inefficiencies and to include non-Gaussian effects like scattering at large angles, bremsstrahlung energy losses and track reconstruction errors.

In chapter 4 I discuss the possibility to find evidence for the existence of supersymmetry with ATLAS. I shortly describe the minimal supersymmetric standard model (MSSM) and the SUGRA model. In the MSSM a complete set of new particles (sparticles) with masses up to about 1 TeV is predicted, including a heavy neutral and stable particle (LSP). Additionally a relatively light Higgs boson of at maximum 135 GeV is predicted. The SUGRA model combines MSSM with supergravity. In this model, all masses and couplings of the sparticles can be calculated from five parameters. The ATLAS collaboration studies five points in the SUGRA parameter space in more detail.

I have compared the production cross-sections of supersymmetric events for these five points studied as calculated with different models and programs (PYTHIA, ISAJET and PROSPINO). I have found that the programs and models currently available can give significantly different results for the production cross-sections of supersymmetric events but that the order of magnitude agrees. Next-to-leading order contributions to the production cross-section can be significant, but in most models only leading order contributions are taken into account. There is a strong correlation between the masses of the sparticles and the corresponding production cross-sections.

I have calculated the response of the ATLAS detector to supersymmetric events for the five SUGRA points using the software package ATLFAST and I have made a signal to background analysis. This study shows that a large missing transverse energy and several hard jets are the clearest signatures of a supersymmetric event. I suggest some preliminary cuts to improve the signal to background ratio. Further studies with larger background samples are however necessary to obtain accurate results.

I have calculated the production cross-sections and the masses of the sparticles as function of the SUGRA parameters and could show that the SUGRA parameter $m_{\frac{1}{2}}$ predominantly determines the production cross-section. At $m_{\frac{1}{2}} = 100$ GeV the total supersymmetric production cross-section is more than 10^6 times larger than at $m_{\frac{1}{2}} = 1500$ GeV.

Chapter 5 focuses on the ATLAS trigger and data acquisition system. The task of the ATLAS trigger system is the online selection of events probably containing an interesting collision. In general only data from those events will be permanently stored for further offline analysis. The ATLAS trigger system consists of three levels: the first level trigger (LVL1), the second level trigger (LVL2) and the event filter.

In the first level trigger the event rate is reduced from 40 MHz to at maximum 100 kHz. Regions of the detector probably containing interesting information that need to be analysed further by the second level trigger are defined (RoIs). In the first level trigger only coarse granularity data from the calorimeter and muon spectrometer is used. Detector data belonging to the events passing the first level trigger is sent to readout buffers (ROBs) via dedicated readout drivers (RODs).

In the second level trigger the event rate is reduced from a maximum of 100 kHz to about 1-5 kHz. The full precision data of all detector components is used. In general only data corresponding to the RoIs defined by the first level trigger system is analysed. The second level trigger handles each detector component separately. During the second level trigger decision the data of the complete ATLAS detector is kept in the ROBs.

In the event filter the event rate is further reduced to about 100 Hz. This results in a requirement to store about 10-100 MB/s permanently. In the event filter the full precision data of the complete ATLAS detector is used. The algorithms implemented will be similar to the algorithms used for the offline analysis, however with looser cuts.

I discuss several options for the architecture of the second level trigger system in chapter 5. I shortly describe a small-scale prototype of the second level trigger system based on the TMS320C40 DSP (Digital Signal Processor) from Texas Instruments.

Finally I present results of calculations of the number of inner detector ROBs per RoI and per event that receive a request (RoI request) to supply data for analysis by the second level trigger system. This number has an important effect on the performance of the second level trigger system. To calculate the results presented in this chapter, I have written the software package MAPPER. I compare two different schemes of mapping the detector modules of the barrel SCT to the ROBs: a regular scheme and an irregular scheme found with Monte Carlo optimisation. I have investigated the influence of taking into account the length of the LHC interaction region along the beam axis in the definition of an RoI. I have shown that this influence can be significant. With the most recent definition of the possible RoI positions and sizes, the regular mapping scheme gives a better result than the mapping scheme found with Monte Carlo optimisation.

In chapter 6 I present a pre-processing algorithm for the precision tracker (SCT plus possibly the pixel detector) data. This algorithm is integrated in the software package SCTFEX, together with the track reconstruction algorithm described in chapter 7.

Pre-processing consists of the transformation from the hits in the format received from the RODs into a format suitable for the track reconstruction algorithm of the second level trigger, i.e. (ϕ, r, z) co-ordinates (space-points). The pre-processing algorithm presented consists of four parts: the selection of hits from detector modules within the current RoI, the combination of hits into clusters, the creation of space-points based on the clusters and the selection of space-points belonging to the RoI (optionally). For each processing step I present results of timing measurements and a parameterisation of these results.

I have investigated the effect of using the pixel detector data in the second level trigger. The calculation time increases significantly when pixel detector data is used. This is mainly due to the complicated cluster reconstruction algorithm. Without the pixel detector (SCT only), 90% of the events can be processed in less than 225 μs (400 MHz Pentium II). When pixel detector data is used in the second level trigger, the 90% point increases to 650 μs .

In the last step of the pre-processing algorithm (selection of space-points belonging to the RoI) about 50% of the space-points created by background tracks can be rejected for the data samples currently available while keeping a good efficiency for space-points created by high- p_T tracks. However more detailed studies with larger data samples in which the length of the LHC interaction region along the beam axis is correctly taken into account are necessary.

In chapter 7 I present a second level trigger algorithm for reconstruction of tracks in the precision tracker. The algorithm consists of histogramming followed by a combinatorial least square fit using data in the selected histogram bins. I have studied the compatibility of the track parameters with the properties of the calorimeter clusters found by the second level trigger calorimeter algorithm. The influences of bremsstrahlung energy losses and detector inefficiencies are ignored in the current algorithm. Tracks are assumed to be straight lines in the (r, ϕ) plane, the (z, ϕ) plane and the (z, r) plane.

I have investigated the effect of using the pixel detector data in the second level trigger, the effect of the values used for several parameters and the effect of variations in the algo-

Summary

rithm on both the physics performance and calculation times. I have shown that both the physics performance and the calculation time increase significantly when the second level trigger uses also the pixel detector data. Especially the reconstruction efficiency for high- p_T tracks is significantly better when the pixel detector data is used. I could show that a high- p_T electron efficiency of about 90% at a jet rejection of 10 can be achieved. Depending on the algorithm options and parameters an average calculation time of less than 10 ms was found on a 400 MHz Pentium II.

Finally I compare the track reconstruction algorithm presented in this chapter with the algorithm that has been used to produce the results presented in the inner detector Technical Design Report (TDR) and with the offline algorithm XKALMAN.

Samenvatting

In dit proefschrift beschrijf ik een studie betreffende de kwaliteit van fysica onderzoek dat met de ATLAS detector mogelijk is en een studie van aspecten van de tweede niveau trigger voor de ATLAS inner detector. In het bijzonder heb ik een parametrisatie van de kwaliteit van spoorreconstructie voor muonen als functie van de pseudorapidity η en transversale impuls p_T en een algoritme voor spoorreconstructie voor de tweede niveau trigger met hoge p_T geladen deeltjes bestudeerd. Bovendien presenteer ik resultaten van studies van het signaal in de ATLAS detector ten gevolge van supersymmetrische interacties en berekeningen van werkzame doorsneden voor de productie van supersymmetrische deeltjes.

In hoofdstuk 1 behandel ik kort het standaardmodel van de deeltjesfysica (SM). Ik beschrijf de belangrijkste eigenschappen van de Large Hadron Collider (LHC) en de mogelijkheid om met de LHC nieuwe fysica te ontdekken. De LHC is een op CERN te bouwen 14 TeV proton-proton collider met een ontwerpluminositeit $L_{design} = 10^{34} \text{ cm}^{-2}\text{s}^{-1}$. Het tijdsinterval tussen twee botsingen bedraagt 25 ns. LHC zal volgens planning in 2005 operationeel worden.

Het belangrijkste onderwerp van onderzoek met LHC is het zoeken naar en bepalen van de eigenschappen van het Higgs boson in het massa gebied van ongeveer 80 GeV tot ongeveer 1 TeV. Behalve de bestudering van Higgs fysica maakt de LHC ook een gedetailleerde studie van het bottomquark en topquark mogelijk. Mogelijke uitbreidingen van het standaardmodel, zoals supersymmetrie (SUSY), kunnen op hun geldigheid worden getest.

In hoofdstuk 2 introduceer ik het ATLAS experiment, een van de vier toekomstige LHC experimenten. Gezien vanuit het botsingspunt is de ATLAS detector opgebouwd uit detectoren voor het reconstrueren van sporen (inner detector), gevolgd door calorimeters en opnieuw detectoren voor het reconstrueren van sporen (muon spectrometer). Detectoren voor het reconstrueren van sporen meten de positie van een passerend geladen deeltje met minimale verstoring. Calorimeters absorberen de meeste deeltjes. De energieën, locaties en bewegingsrichting van deze deeltjes kunnen worden gemeten omdat een gedeelte van de gedeponeerde energie geconverteerd wordt in licht of lading. De complete inner detector is geplaatst in een magnetische solenoïde met een centrale veldsterkte van 2T en een afbuigvermogen van 2.1 Tm. De muon spectrometer is geplaatst in het magnetische veld van een toroïde met een afbuigvermogen van 3-6 Tm. De gehele ATLAS detector is verdeeld in een centraal gedeelte, waar detectielagen op cilindrische oppervlakken rond de bundelas zijn geplaatst, en twee eindstukken, waar detectielagen loodrecht op de bundelas zijn geplaatst.

In dit hoofdstuk bespreek ik kort het magneetsysteem van ATLAS, het calorimetersysteem en de muon spectrometer. De inner detector bespreek ik in meer detail. De inner detector bestaat uit pixeldetectors en microstripdetectors (SCT) van silicium met een hoge resolutie het dichtst bij het interactiepunt en detectoren voor continue spoorreconstructie (TRT) aan de buitenkant.

In hoofdstuk 3 presenteer ik een parametrisatie van de nauwkeurigheid waarmee sporen van muonen in de ATLAS inner detector kunnen gereconstrueerd. Deze parametrisatie wordt gebruikt in het software pakket ATLFAST. Voor een gegeven set van parameters, die het spoor van een muon in het magneetveld van de inner detector beschrijven, kan een uitgesmeerde set van parameters worden berekend, die representatief zijn voor echte metingen. Hierbij wordt de invloed van de intrinsieke resolutie van de detectoren, veelvoudige verstrooiing en de correlatie tussen de spoorparameters in rekening gebracht.

Ik heb de nauwkeurigheid waarmee de spoorparameters bepaald kunnen worden en hun correlaties als functie van de pseudorapidity η en de transversale impuls p_T bepaald. De invloed van verschillende modellen die gebruikt kunnen worden voor het magneetveld waarin de inner detector is geplaatst en de invloed van de aanwezigheid en gebruik van data van de eerste pixellaag (B-laag) op de nauwkeurigheid heb ik onderzocht. Aan de hand van deze parametrisatie heb ik de spoorreconstructie op basis van data van de gecombineerde inner detector/muon spectrometer en de waarschijnlijkheid van correcte identificatie van de lading van muonen bestudeerd. Tenslotte beschrijf ik kort mogelijke methoden om de parametrisatie uit te breiden om voor elektronen en pionen van belang zijnde niet Gaussische effecten zoals verstrooiing over grote hoeken, energieverliezen ten gevolge van bremsstrahlung en fouten in de spoorreconstructie in rekening te brengen en om in rekening te brengen dat niet alle sporen worden gereconstrueerd.

Hoofdstuk 4 heeft als onderwerp hoe het bestaan van supersymmetry met ATLAS aangevoeld zou kunnen worden. Het minimale supersymmetrische standaardmodel (MSSM) en het SUGRA model beschrijf ik kort. In het MSSM wordt een complete set van nieuwe deeltjes met massa's tot ongeveer 1 TeV voorspeld, inclusief een zwaar neutraal en stabiel deeltje (LSP). Bovendien wordt een relatief licht Higgs boson van maximaal 135 GeV voorspeld. Het SUGRA model combineert MSSM met supergravity. In dit model kunnen alle massa's en koppelingen van de supersymmetrische deeltjes worden berekend aan de hand van vijf parameters. Vijf punten in de SUGRA parameterruimte worden in meer detail bestudeerd door de ATLAS groep.

Ik heb de werkzame doorsneden voor de productie van supersymmetrische deeltjes voor de bestudeerde vijf punten en berekend met verschillende modellen en programma's (PYTHIA, ISAJET, PROSPINO) vergeleken. Ik heb gevonden dat de op dit moment beschikbare programma's en modellen significant verschillende resultaten kunnen geven voor de supersymmetrische wisselwerking maar dat de orde van grootte van de werkzame doorsneden overeenkomt. Hogere orde bijdragen kunnen significant zijn terwijl in de meeste modellen alleen de eerste orde bijdragen worden meegenomen. Er bestaat een sterke correlatie tussen de massa's van de supersymmetrische deeltjes en de bijbehorende werkzame doorsneden voor de productie van deze deeltjes.

Het signaal in de ATLAS detector ten gevolge van een supersymmetrische wisselwerking voor de vijf bestudeerde SUGRA punten heb ik berekend met het softwarepakket ATLFAST en vergeleken met het signaal ten gevolge van achtergrondinteracties. Deze studie toont aan dat een grote missende transversale energiecomponent en verscheidene harde jets de duidelijkste aanwijzing voor een supersymmetrische wisselwerking zijn. Ik suggereer een aantal voorlopige selectiecriteria om de signaal/achtergrondverhouding te verbeteren. Verdere studies met grotere achtergrondsamples zijn echter noodzakelijk.

Ik heb de werkzame doorsneden voor de productie van supersymmetrische deeltjes en de massa's van deze deeltjes als functie van de SUGRA parameters berekend. Ik heb aangetoond dat de werkzame doorsneden voornamelijk bepaald worden door de SUGRA parameter $m_{1/2}$. Voor $m_{1/2} = 100$ GeV is de totale werkzame doorsnede voor de productie van supersymmetrische deeltjes meer dan een factor 10^6 groter dan voor $m_{1/2} = 1500$ GeV.

Hoofdstuk 5 heeft als onderwerp het trigger en data acquisitie systeem van ATLAS. De taak van het ATLAS trigger systeem is het online selecteren van gebeurtenissen waarvoor mogelijk een interessant botsingsproces is opgetreden. In het algemeen zullen alleen de data behorende bij deze gebeurtenissen permanent worden opgeslagen voor verdere offline

analyse. Het ATLAS trigger systeem bestaat uit drie niveau's: de eerste niveau trigger (LVL1), de tweede niveau trigger (LVL2) en het event filter.

In de eerste niveau trigger wordt het aantal gebeurtenissen per seconde teruggebracht van 4×10^7 tot maximaal 1×10^5 . Gebieden van de detector die waarschijnlijk interessante informatie bevatten die verder geanalyseerd moeten worden door de tweede niveau trigger worden gedefinieerd (RoIs). De eerste niveau trigger maakt alleen gebruik van data van de calorimeter en muon spectrometer met een lage resolutie. De data van de detector die behoren bij gebeurtenissen welke door de eerste niveau trigger geaccepteerd worden, worden via de "readout drivers" (RODs) naar de "readout buffers" (ROBs) getransporteerd.

In de tweede niveau trigger wordt het aantal gebeurtenissen per seconde verder teruggebracht van 1×10^5 tot ongeveer $1-5 \times 10^3$. De data van alle detectorcomponenten worden gebruikt. In het algemeen worden alleen de data behorend tot RoIs die gedefinieerd zijn door de eerste niveau trigger geanalyseerd. Elke detectorcomponent wordt afzonderlijk behandeld in de tweede niveau trigger. De data van de complete ATLAS detector worden bewaard in de ROBs tijdens het nemen van de tweede niveau triggerbeslissing.

In het event filter wordt het aantal gebeurtenissen per seconde verder teruggebracht tot ongeveer 100. Dit betekent dat ongeveer 10-100 MB/s permanent opgeslagen moet kunnen worden. In het event filter worden de data van de complete ATLAS detector gebruikt. De gebruikte algoritmen zullen lijken op de algoritmen die gebruikt worden voor de offline analyse, er zullen echter minder stringente selectiecriteria gebruikt worden.

Ik behandel in hoofdstuk 5 verscheidene opties voor de architectuur van het tweede niveau trigger systeem. Ik beschrijf kort een kleinschalig prototype van het tweede niveau trigger systeem, waarin gebruik gemaakt is van de TMS320C40 DSP (Digitale Signaal Processor) van Texas Instruments.

Het aantal ROBs dat per RoI en per gebeurtenis een verzoek (RoI request) ontvangt om data te leveren voor analyse door de tweede niveau trigger heb ik berekend voor de inner detector. Dit aantal heeft een belangrijke invloed op de prestatie van het tweede niveau trigger systeem. Om de resultaten die in dit hoofdstuk gepresenteerd worden te kunnen berekenen heb ik het softwarepakket MAPPER geschreven. Ik vergelijk twee verschillende schema's om de detector modules van het centrale gedeelte van de SCT in ROBs in te delen: een regelmatig schema en een onregelmatig schema gevonden met behulp van Monte Carlo optimalisatie. De invloed van het in rekening brengen van de lengte van het LHC interactiegebied parallel aan de bundelas in de definitie van een RoI heb ik onderzocht. Ik heb aangetoond dat deze invloed significant kan zijn. Met de meest recente definitie van de mogelijke RoI posities en groottes geeft het regelmatige indelingsschema een beter resultaat dan het indelingsschema gevonden met behulp van Monte Carlo optimalisatie.

In hoofdstuk 6 presenteer ik een voorbehandelingsalgoritme voor de data van de precisie tracker (SCT plus eventueel de pixel detector). Dit algoritme is geïntegreerd in het softwarepakket SCTFEX, samen met het spoorreconstructie algoritme dat beschreven wordt in hoofdstuk 7.

Voorbehandeling bestaat uit de transformatie van de hits in het formaat ontvangen van de RODs naar een formaat geschikt voor het spoorreconstructie algoritme van de tweede niveau trigger, namelijk (ϕ, r, z) coördinaten. Het gepresenteerde algoritme bestaat uit vier delen: de selectie van hits afkomstig van modules die binnen de huidige RoI vallen, de combinatie van hits tot clusters, het maken van punten in de driedimensionale (ϕ, r, z) ruimte gebaseerd op de clusters en de selectie van de punten die tot de RoI behoren (optioneel). Voor elke stap presenteer ik resultaten van tijdmetingen en een parametrisatie van deze resultaten.

Het effect van het gebruik van de data van de pixeldetector in de tweede niveau trigger heb ik onderzocht. De verwerkingstijd neemt significant toe als de data van de pixeldetector worden gebruikt in de tweede niveau trigger, hoofdzakelijk ten gevolge van het gecompliceerde algoritme voor het reconstrueren van clusters. Zonder pixeldetector (alleen SCT) is de verwerkingstijd voor 90% van de gebeurtenissen korter dan 225 μs (400 MHz Pentium II). Met de pixeldetector is de verwerkingstijd voor 90% van de gebeurtenissen korter dan 600 μs .

In de laatste stap van het voorbehandelingsalgoritme (selectie van punten die tot de RoI behoren) wordt voor de huidige datasamples ongeveer 50% van de punten gecreëerd door achtergrond niet geselecteerd, terwijl een goede efficiëntie voor punten veroorzaakt door hoge p_T sporen behouden blijft. Gedetailleerdere studies met grotere datasamples waarbij de lengte van het LHC interactiegebied langs de bundelas correct in rekening wordt gebracht, zijn echter noodzakelijk.

In hoofdstuk 7 presenteer ik een spoorreconstructie algoritme voor de precisie tracker dat gebruikt kan worden in de tweede niveau trigger. Het algoritme bestaat uit het maken van een histogram en een kleinste kwadraten fit over alle mogelijke combinaties in de geselecteerde bins van het histogram. Ik heb de compatibiliteit onderzocht van de parameters van het reconstrueerde spoor met de eigenschappen van de calorimeterclusters, gevonden met het tweede niveau trigger calorimeter algoritme. De invloeden van energieverliezen ten gevolge van bremsstrahlung en van het feit dat de detector niet 100% efficiënt is worden verwaarloosd in het huidige algoritme. Er wordt aangenomen dat sporen bestaan uit rechte lijnen in het (r, ϕ) vlak, het (z, ϕ) vlak en het (z, r) vlak.

Ik heb de invloed van het gebruik van de data van de pixeldetector in de tweede niveau trigger, de invloed van de waardes die gebruikt worden voor verschillende parameters en de invloed van variaties in het algoritme op zowel het vermogen om sporen te reconstrueren als de rekestijden onderzocht. De waarschijnlijkheid van correcte identificatie en nauwkeurige reconstructie van sporen en de benodigde rekestijd nemen significant toe als de data van de pixeldetector worden gebruikt in de tweede niveau trigger. Bij gebruik van de data van de pixeldetector wordt ongeveer 90% van de hoge p_T elektronen geselecteerd, samen met een reductie van ongeveer een factor 10 van de achtergrond. Afhankelijk van de gebruikte opties voor het algoritme en waardes voor de parameters kan een gemiddelde rekestijd van minder dan 10 ms worden bereikt op een 400 Mz Pentium II.

Tenslotte vergelijk ik het in dit hoofdstuk gepresenteerde algoritme voor het reconstrueren van sporen met het algoritme dat gebruikt is om de in het Technisch Design Rapport (TDR) voor de inner detector gepubliceerde resultaten te produceren en met het offline algoritme XKALMAN.